SPATIALLY RESOLVED ACOUSTIC AND AERODYNAMIC STUDIES UPSTREAM AND DOWNSTREAM OF AN INDUSTRIAL AXIAL FAN WITH INVOLVEMENT OF THE PHASED ARRAY MICROPHONE TECHNIQUE

T. Benedek – J. Vad

Department of Fluid Mechanics, Faculty of Mechanical Engineering
Budapest University of Technology and Economics (BME)
Bertalan Lajos u. 4 - 6., H-1111 Budapest, Hungary. Email: vad@ara.bme.hu

ABSTRACT

The paper presents the further development of a combined acoustic-aerodynamic diagnostics method, suited to on-site investigation of industrial axial fans. The method, involving phased array microphone experiments, has been demonstrated in a case study. The acoustic data have been processed by means of a Rotating Source Identifier algorithm, and represented in the form of upstream and downstream source maps. A procedure has been reported for investigating the effect of duration of averaging on the phased array microphone results. A supplementary experiment has been elaborated for elimination of noise source ambiguity in evaluating the source maps. Certain rotor noise sources have been localised in a detailed manner. The momentum thickness parameter has been introduced and experimentally justified as a representative indicator of both aerodynamic loss and upstream-radiated noise. This offers a basis for fan redesign for reducing both noise and loss.

NOMENCLATURE

A_1, B_1, A, B parameters used in theoretical approximation of L_{PM} by L_{Pl}
c blade chord
c_t blade chord at tip
D Lieblein diffusion factor
d_t tip diameter
f_{mid} middle frequency of frequency band studied
F normalized wake momentum thickness = θ / c
H shape factor
L_P local sound pressure level
L_{Pl} theoretical approximation of L_{PM} as function of θ^*
L_{PM} level of circumferential average of measured P values
L_{θ^*} momentum thickness level
ΔL_P level difference for subtractive source maps and for their circumferential average
P measured local sound pressure, normalized by a reference value
P_M circumferential area-average of measured P values
P_1 approximation of P_M as function of θ^*
R dimensionless radius (radius normalized by tip radius)
S characteristic size of the PAM
S_{RES} spatial resolution of the PAM measurement at a given wavelength
Z distance between the PAM and the plane of investigation
δ displacement thickness of the boundary layer
θ momentum thickness of the boundary layer
θ^* momentum thickness parameter $=100\cdot(c/c_t)\cdot F(D)$
λ wavelength, corresponding to f_{mid}
Φ flow coefficient (annulus area-averaged axial velocity normalized by tip circumferential speed)

1. INTRODUCTION AND OBJECTIVES

Any axial flow fan in an industrial environment may exhibit aerodynamic as well as acoustic behaviour being different from that suggested by the measurement data specified in the fan catalogue, obtained under laboratory circumstances. For example, due to the environment of the installed fan, the inlet flow to the rotor may significantly differ from the inlet condition assumed in design or realized in the performance curve measurements. As a consequence, the operating point may depart from the characteristic curve, and the fan may produce increased aerodynamic loss and noise. In order to elaborate remedial techniques against such unfavourable behaviour, the on-site, concerted acoustic-aerodynamic investigation of the criticised fans is of practical importance.

Phased array microphone (PAM) systems operate on the basis of the beamforming methodology, in which the phase difference between the signals of multiple microphones is utilized to estimate the direction of arrival of the wave fronts. The PAM technique offers a State-of-the-Art means for localization and identification of turbomachinery noise sources. It gives a potential for making a distinction between fan noise and other noise components, appearing e.g. as background noise in industrial fan applications. For localization of rotating noise sources in acoustic diagnostics of fan rotors, the application of the Rotating Source Identifier (ROSI) PAM data processing algorithm, being an extension of the beamforming methodology, is beneficial (Sijtsma et al., 2001). PAM experimentation [a] adapted to on-site surveillance, [b] suited to industrial fans, [c] supported by the ROSI algorithm, and [d] supplemented with spatially resolved aerodynamic measurements is therefore a powerful tool in combined acoustic-aerodynamic diagnostics of industrial fans. However, as the literature suggests, the experiences are still limited in this field. [a] PAM is mostly applied to axial flow turbomachinery in laboratory experiments (Lowis and Joseph, 2006; Podboy and Horváth, 2009; Sijtsma, 2010; Minck et al., 2012; Horváth et al., 2014), and the applied PAM is often an immobile device. [b] The subjects of the studies are mostly not industrial fans but aero-engine fans (Podboy and Horváth, 2009; Sijtsma, 2010; Ji et al., 2013; Kennedy et al., 2013; Horváth et al., 2014). [c] The ROSI algorithm is still seldom applied (Sijtsma et al., 2001; Sijtsma, 2010). [d] Very few experimental papers report on *spanwise-resolved* fan noise data, and discussing their possible correlation with spatially resolved aerodynamic features (Bianchi et al., 2009, 2011).

In order to completely satisfy the need formulated in points [a] to [d], the authors established a combined acoustic-aerodynamic diagnostics technique, and demonstrated its capabilities in a case study (Benedek and Vad, 2014). Spanwise distributions of loss indicators related to the blading as well as those of the PAM-measured sound pressure were simultaneously studied.

The present paper reports on further developing and extending the diagnostics methodology reported in the ASME Paper GT2014-25916 by Benedek and Vad (2014). This reference provides further details on the instrumentation, limitations and measurements errors, data processing and evaluation methods, as well as on the case study fan, its operational parameters, aerodynamic features and geometrical details. The same fan case study is discussed herein. The upstream (US) PAM experiments are supplemented with downstream (DS) measurements. Novel elements of the data acquisition, processing, and evaluation technique are reported. A new indicator is introduced for an empirical correlation between local noise and aerodynamic loss along the span. Such correlation serves with guidelines in redesigning the fan for simultaneous reduction of noise and loss.

2. FAN OF CASE STUDY, EXPERIMENTAL TECHNIQUE

The fan is a rotor-only configuration with forward-skewed blades, built in a short duct, and equipped with a short inlet cone. It is a wall-mounted free-inlet, free-exhausting ventilating fan. The main data of the fan are as follows. Tip diameter: $d_t = 300$ *mm*, hub-to-tip diameter ratio: 0.30, tip clearance relative to the span: 0.066, rotor speed: 1430 *RPM*, flow coefficient: $\Phi = 0.316$. The axial velocity profile inlet to the fan was measured by means of a vane anemometer probe. The scheme of the PAM measurements is presented in Figure 1. The schematic view of the rotor is illustrated in Figure 2 in the PAM source maps. The five rotor blades are drawn in the maps in correspondence

with the angular position of the rotor. The rotor annulus area is indicated in the maps using concentric circles (inner circle: at the hub of $R = 0.30$; outer circle: at the tip of $R = 1.00$).

The acoustical measurements were performed using a general purpose Optinav Inc. Array 24 portable PAM system, having 24 microphones sunk into an octagonal aluminium plate along a logarithmic spiral curve. The diameter of the circle enveloping the octagonal plate is 3.17 d_t. The PAM plate was set perpendicular to the axis of rotation, and the centre of the array coincided with the rotor axis. As Fig. 1 shows, the array was placed at a distance of 1.83 d_t from the inlet plane of the fan casing for the US measurements. For the DS measurements, the distance between the outlet plane of the fan casing and the array was increased by a factor of 2 (to 3.66 d_t), in order to avoid the overload of the microphones. The modification of the distance resulted in a reduction in the detected DS sound pressure, which was compensated in processing the data.

During the US as well as the DS measurements, the loading state of the microphones was continuously monitored. By such means, the saturation of the microphones has securely been avoided. In spite of the carefulness in executing the measurements, Mueller et al. (2002) draws the attention that spurious microphone overloads occur by chance, contributing to the error of the phased array calculation. Therefore, the microphone signals were subjected to a repeated check prior to post-processing. Only a portion of 10^{-7} of the measurement signals was found to be saturated. Based on the quantification in Mueller et al. (2002), the error due to such spurious overloads was considered negligible in the present case study.

Due to the absence of outlet guide vanes, the air jet generated by the fan is swirling, and, as such, is highly divergent. Still, the airflow impacts on the PAM device to a certain extent in the DS measurements. The pseudo-sound associated with the turbulent pressure fluctuations is detected by the microphones. The source maps are computed via correlating the microphone signals with the premise that the waves propagate at the speed of sound. Since the pseudo-sound propagates at a substantially different speed, i.e. in a convective manner (Ristrorcelli, 1997), it remains disregarded in the correlation technique. However, it contributes to the amplitude uncertainty of the measurements. The amplitude uncertainty of the PAM measurements has been estimated herein to be ± 1.0 dB.

The spatial resolution is the shortest distance within which two sources can be distinguished on the source maps. It is estimated theoretically with use of the following formula (Hald, 2005):

$$S_{RES} = 1.22 \cdot \lambda \cdot Z / S \qquad (1)$$

Circles are presented on the top left corner of the US source maps in Fig. 2, the diameter of which corresponds to S_{RES} for the US measurements. For the DS measurements, the spatial resolution has been deteriorated – i.e. S_{RES} has been increased – by a factor of 2, in comparison to that of the US measurements at a given λ, since Z was increased by a factor of 2.

The angular position of the rotor, being necessary for the ROSI algorithm, was detected by means of a non-contact encoder adaptable to on-site studies. The uncertainty of the angular position of the rotor is estimated conservatively to be $\pm 2.5°$. A sampling frequency of 44100 Hz has been applied, being the maximum frequency made available by the data acquisition system. The PAM-based, spatially resolved results presented in the paper originate from capturing and averaging the acoustic data for 20 s, i.e. for ≈ 480 rotor revolutions. Section 4 is referred to for further details.
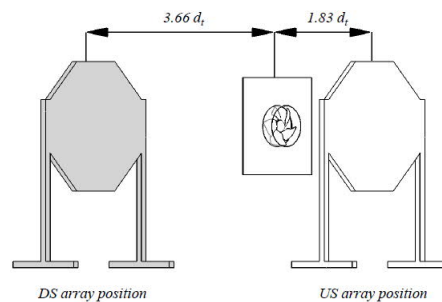

Figure 1. Schematic view of the PAM measurements

3. PAM SOURCE MAPS; ASPECTS OF EVALUATION

The PAM-based noise spectra are presented in Benedek and Vad (2014). As discussed there in detail, the fan noise is dominated by broadband noise sources. For obtainment of the source maps, the third-octave frequency bands of f_{mid} = 2000, 2500, 3150, 4000, 5000, and 6300 Hz have been selected. Fig. 2 presents the US (left column) and DS (middle column) source maps. The maps correspond to an inspection area of 0.5 m X 0.5 m, having the rotor in the centre. Taking the classification in Carolus (2003) and in De Gennaro and Kuehnelt (2012) as a basis, PAM experiments may aim at identifying the following potential broadband noise sources related to the rotor.

- *Turbulence ingestion noise* ← Turbulent inflow originating from the inlet cone at the highest radii, and impacting on the leading edge;
- *Boundary layer noise* ← Interaction of the turbulent boundary layer with the blade surface;
- *Trailing edge noise* ← Interaction of the turbulent boundary layer with the trailing edge;
- *Vortex shedding noise* ← Interaction of the boundary layers just downstream of the trailing edge (partly broadband noise source);
- *Separation noise* ← Boundary layer separation, near the leading edge, or further downstream;
- *Tip leakage flow noise* ← Turbulent tip leakage flow.

In order to quantify the radial distribution of rotor noise, the P data in the US as well as DS source maps have been area-averaged along the circumference (conf. Vad and Benedek, 2014), resulting in $P_M(R)$ profiles. The $P_M(R)$ distributions are presented in the right column of Fig. 2, in the form of logarithmic levels L_{PM}. The hub radius at R = 0.3 is indicated with use of a dashed line. As shown in the figure, the DS-measured P_M data mostly exceed the US-measured noise. This implies that the DS-radiated noise – e.g. trailing edge noise and vortex shedding noise – is significant. However, the spatial resolution for the DS source maps, being deteriorated in comparison to that for the US maps, does not allow the localisation of the DS-radiating sources in this case study.

The $L_{P1}(R)$ distributions for the US measurements, indicated in the right column of Fig. 2 with use of dot symbols, are discussed in Section 6.

4. EFFECT OF DURATION OF AVERAGING

When detecting rotating sources, the duration of averaging is of crucial importance. With regard to the necessary duration of averaging the PAM data – or, analogously, to the necessary number of rotor revolutions for averaging –, the literature is very limited. Such information is rare, is restricted to the conventional Delay & Sum algorithm capable for detecting standing sources, and is specified for particular case studies only, without providing any generally valid guidelines. Data out of such particular cases are as follows, in the following sequence of information: reference / duration of averaging / rotor speed: Ji et al. (2013) / 21 s / RPM not available; Kennedy et al. (2013) / 10 s / 2359 RPM; Horváth et al. (2014) / 45 s / 6590 RPM. No recommendations were found in the literature for the ROSI algorithm with regard to duration of averaging. Therefore, the authors carried out a detailed study in this topic. For investigating the effect of duration of averaging, PAM samples of three different durations were recorded and processed using the ROSI algorithm: 5 s ($\approx$ 120 revolutions), 10 s ($\approx$ 240 revs.), and 20 s ($\approx$ 480 revs.). The discrepancy between the resultant source maps has been found to be negligible in the bands of lower frequencies, up to f_{mid} = 3150 Hz. The bands of higher frequencies ($f_{mid} \geq$ 4000 Hz) have been found as relevant indicators of sensitivity to duration of averaging. The reason is that the noise due to turbulent fluctuations, e.g. noise associated with the turbulent boundary layer (Shin et al., 2007) dominates the bands of higher frequencies, and sufficiently long duration of averaging is needed for a proper representation of the related noise pattern. Therefore, the sensitivity to duration of averaging is demonstrated herein on the band of the highest frequency of f_{mid} = 6300 Hz. Figure 3 presents *subtractive source maps* for this band, generated by subtracting the individual US maps related to the various durations of averaging. The subtractive map of the US source maps of 20 s and 5 s, as well as that of the US source maps of 20 s and 10 s, are shown on the left-hand side and in the middle of Fig. 3, respectively.
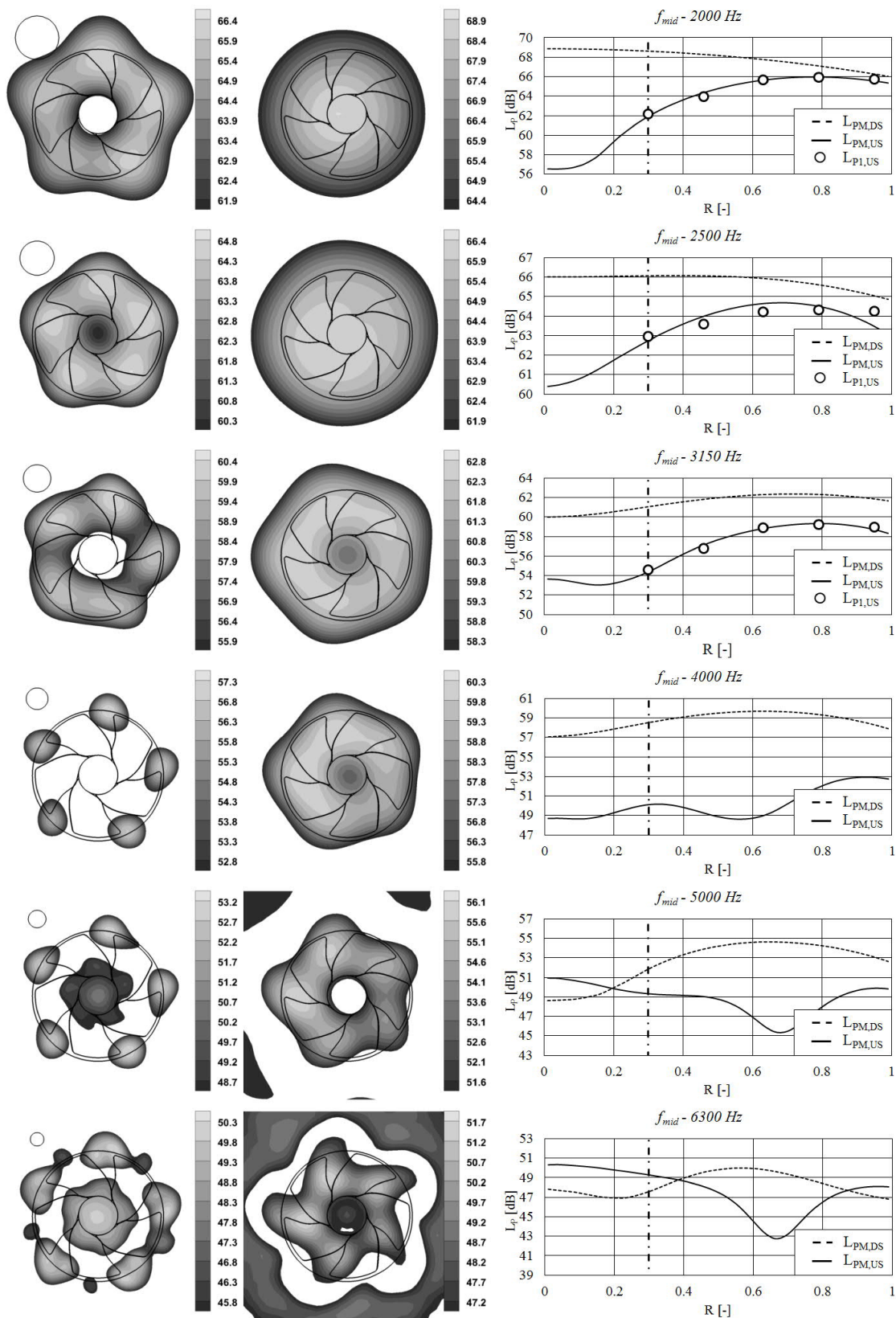
Figure 2. Left column: US source maps with scaling of L_P [dB]. Middle column: DS source maps with scaling of L_P [dB]. Right column: L_{PM} (R) distributions. The spatial resolution S_{RES} for the US source maps corresponds to the diameter of the circles on the top left corner of the US source maps. S_{RES} for the DS source maps: 2 times S_{RES} for the US source maps.

The scale of the maps in Fig. 3 is between -1 and 1 dB, according to the estimated amplitude uncertainty of ± 1 dB of the PAM experiment. The maps suggest that the increase of duration of averaging tends to further increase the maxima and further reduce the minima of the detected sound pressure. The range of the [20s–5s] map exceeds ± 1 dB. However, the range of the [20s–10s] map is already within the range of experimental uncertainty of ± 1 dB. The aforementioned trends are illustrated also by the right-hand side of Fig. 3, where the circumferentially averaged radial profiles of the subtractive source maps are presented. Whereas the [20 s–5s] profile still exceeds the range of experimental uncertainty of ± 1 dB, the [20s–10s] profile is already within that. On this basis, it has been stated that by extending the duration of averaging to 20 s (≈ 480 revs.), an insensitivity of the PAM results has been reached with respect to duration of averaging, within the range of the measurement uncertainty. This justifies the reasonability of presenting and discussing the PAM results related to duration of averaging of 20 s in the paper.
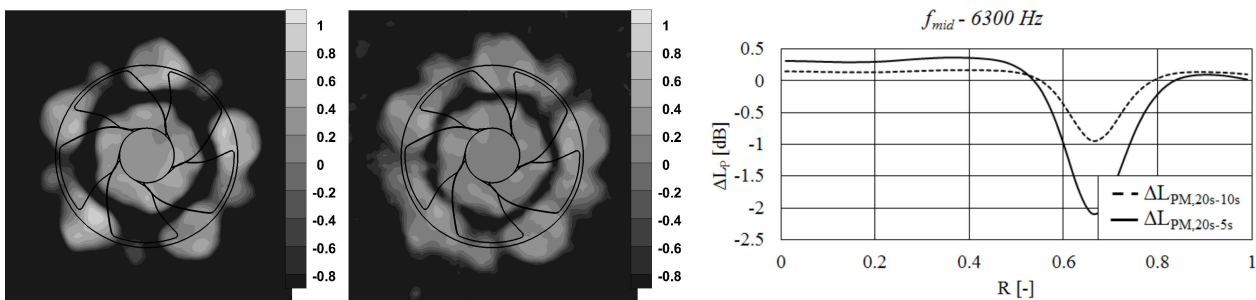

Figure 3. Subtractive US source maps: band of f_{mid} = 6300 Hz. Left: [20s–5s] map (ΔL_P [dB]). Middle: [20s–10s] map (ΔL_P [dB]). Right: ΔL_{PM} (R) distributions for the subtractive maps.

5. ELIMINATION OF NOISE SOURCE AMBIGUITY, EVALUATION OF SOURCE MAPS

As Fig. 2 illustrates, the US source maps show the repetition of the source image patterns – i.e. spots of sound pressure peaks – in the pitchwise direction, in accordance with the periodicity of the rotor blade passages. A similar repetition can be observed on the DS source maps as well, although its visibility is limited due to the moderate spatial resolution of DS detection. From diagnostics point of view, it is essential to discover the dominant noise sources associated with these peaks, for a more comprehensive understanding of the underlying physics of noise generation. However, taking the direction of rotation as a basis, it is ambiguous whether a given noise peak is associated with phenomena related to a) *the blade preceding the peak* – e.g. suction side boundary layer noise or tip leakage flow noise originating from the *preceding* blade –, or b) *the blade following the peak* – e.g. turbulence ingestion noise or separation noise from the leading edge of the *following* blade.

In order to eliminate such ambiguity, the following technique has been proposed as an extension of the presented on-site diagnostics method. A single blade has been elongated, i.e. the tip clearance of it has been reduced to 30 percent of the original value. For this purpose, a narrow cardboard plate has been used, having a camber geometry being identical with that of the blade tip, and firmly stuck to the tip. The plate may cause rotor unbalance and vibration, potentially resulting in tonal noise. By evaluating the PAM-based noise spectra, such additional noise has been found negligible. Furthermore, the following notes are made, on the basis of Daly (1992). The rotor of case study is a narrow impeller (breadth is less than 0.2 d_t). Therefore, it may dominantly have an inclination to static unbalance, characterised by a vibration frequency being equal to the rotational frequency of 24 Hz. The corresponding tonal noise, if any, would fall far from the PAM-investigated frequency bands (the minimum value for f_{mid} is 2000 Hz), and thus, it would not affect the evaluation of PAM results presented herein.

Having the tip clearance reduced by such means, the PAM measurements were repeated. The resultant source maps are presented in Figure 4. The blade of reduced tip clearance is indicated with

arrows in Fig. 4. The source maps of Fig. 4 have been compared to those of Fig. 2 of uniform tip clearance. The comparative source maps are of identical scaling for comparability. The results of the qualitative comparison are summarized in Figure 5. It has been investigated how the reduction of tip clearance influences the value of the sound pressure peaks. (+) and (-) signs in Fig. 5 indicate an amplification or attenuation in the local peak value, respectively. The pitchwise-averaged representative position of the peaks is the mid-pitch position between the blades preceding and following the peak. Therefore, the (+) and (-) signs represent the peaks at mid-pitch position between the leading and trailing edges for the US and DS measurements, respectively.

Only the qualitative changes observed *consequently for each frequency band* are presented in Fig. 5, and are discussed herein. The figure suggests the following qualitative trends → for which the following explanations are provided.

Peak of label 1, Fig. 5: The reduction of tip clearance, i.e. the attenuation of tip leakage flow, tends to attenuate the US noise peak that is *preceded* by blade of reduced clearance. → The peaks in the US source maps are associated with flow phenomena related to the blades *preceding* the peaks. Therefore, the noise sources located near the leading edge of the blades *following* the peaks – such as turbulence ingestion noise, or separation noise – are not dominant. On the basis of the US maps in Fig. 2, the following noise sources can be identified. a) Noise of the boundary layer developing on the suction side of the blade, facing toward the US direction. This noise dominates away from the endwalls on the maps of $f_{mid} \leq 3150$ *Hz*. b) Tip leakage flow noise. This noise dominates near the tip on the maps of $f_{mid} \geq 4000$ *Hz*. As support to this group of maps, e.g. Fukano and Jang (2003) and Corsini et al (2009) confirm that the tip leakage flow noise may dominate within the rotor under certain conditions.

Peak of label 2, Fig. 5: The attenuation of tip leakage flow tends to attenuate also the US noise peak at the *second blade passage following the blade of reduced clearance* . → This symptom is a circumstantial evidence for the presence of the *double leakage* phenomenon. Referring to Khalid et al. (1999), double leakage means that the tip leakage flow intersects the pressure surface of the adjacent blade, and leaks across again. The double leakage phenomenon is considered herein as the exclusive means via which the reduction of tip clearance size impacts on the *second* adjacent blade passage, from aerodynamics as well as from acoustics points of view. In Khalid et al. (1999), the double leakage phenomenon was demonstrated using Computational Fluid Dynamics (CFD) simulations. Based on this guideline, CFD simulations (to be presented in a future paper) were carried out also on the rotor of case study. These CFD studies confirmed the presence of the double-leakage phenomenon in the rotor. As an extension to the noise class of tip leakage flow noise, the concept of *double-leakage flow noise* is therefore introduced herein. By attenuating the tip leakage flow (due to reduction of tip clearance size), the double-leaked flow also attenuates, leading to local noise reduction in the *second* adjacent blade passage.

The following detected trends require further investigations for explanation.

Peak of label 3, Fig. 5: The reduction of tip clearance tends to amplify the US noise peak at the blade passage *preceding* the blade of reduced clearance.

Peak of label 4, Fig. 5: The reduction of tip clearance tends to amplify the DS noise peak that is *preceded* by blade of reduced clearance.

6. CORRELATION BETWEEN ROTOR NOISE AND AERODYNAMIC LOSS

The objective of this section is the establishment of semi-empirical redesign guidelines for simultaneous reduction of rotor noise and loss. In Benedek and Vad (2014), the geometrical and aerodynamic data of the case study rotor along the span are discussed in detail. As further development of the concept described there, a cascade loss indicator is introduced herein, offering a possibility for correlation between flow-induced noise and aerodynamic loss. The spanwise distributions of c and D are taken from Benedek and Vad (2014) for the calculation example discussed at the end of this section.
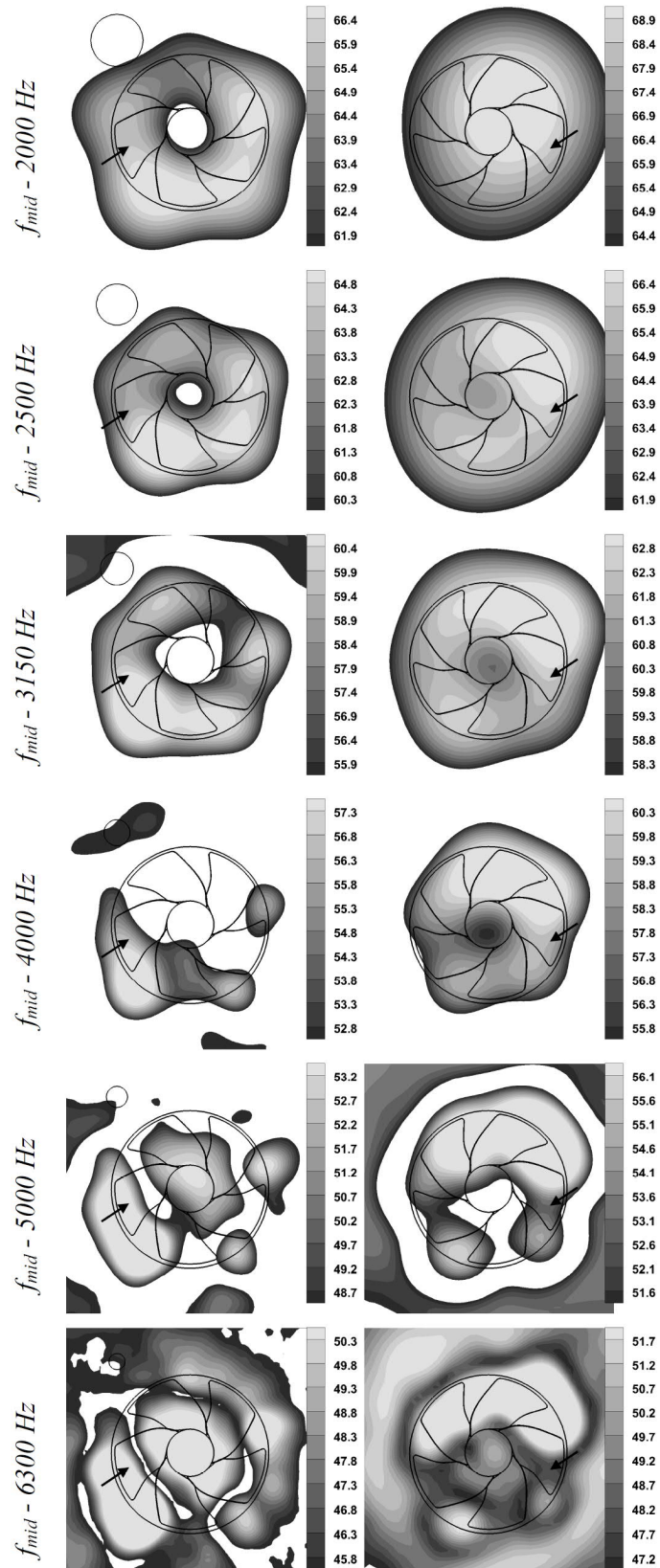
Figure 4. Effect of reduced tip clearance. The blade of reduced tip clearance is indicated by arrows. Left column: US source maps with scaling of L_P [dB]. Right column: DS source maps with scaling of L_P [dB]. The spatial resolution S_{RES} for the US source maps corresponds to the diameter of the circles on the top left corner of the US source maps. S_{RES} for the DS source maps: 2 times S_{RES} for the US source maps.
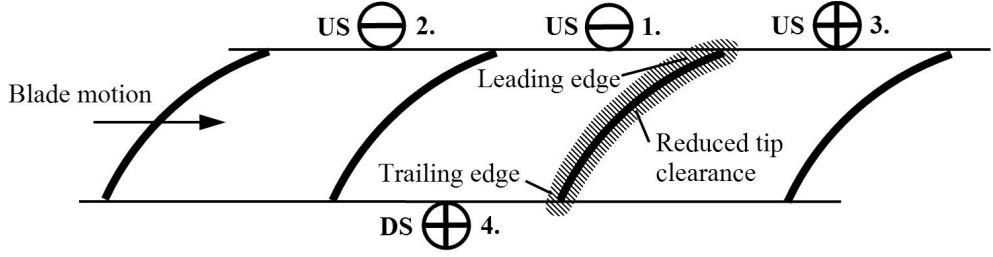
Figure 5. Sketch for the detected effects due to tip clearance reduction

As suggested by the theory detailed in De Gennaro and Kuehnelt (2012), it is generally assumed that the pressure of radiated noise is proportional to the displacement thickness of the blade boundary layer at the trailing edge – being approximately equal to the displacement thickness in the wake: $P \propto \delta$. Based on Lakshminarayana (1996), the shape factor is defined as $H = \delta/\theta$. According to Lieblein (1965), H is usually less than 1.2 in conventional unstalled configurations, and therefore, H is approximated briefly herein as unity. The above read the following approximation:

$$P \propto \theta \tag{2}$$

Lieblein (1965) established a strong correlation between the D diffusion factor and the wake momentum thickness θ normalized by the blade chord c. In Vad (2011), the following empirical formula has been proposed for this correlation:

$$\theta/c = F(D) = 6.2 \cdot 10^{-3} + 3 \cdot 10^{-4} \cdot \exp(6.34 \cdot D) \tag{3}$$

With use of Eq. (3), the normalized momentum thickness F is obtained as function of D, and the wake momentum thickness is calculated as $\theta = c \cdot F(D)$. Substituting this formula into Eq. (2) reads the correlation $P \propto [c \cdot F(D)]$. With the knowledge of the spanwise distribution of the c and D characteristics, the $\theta(R) = [c \cdot F(D)](R)$ profile can be calculated for the rotor. In order to make possible a non-dimensional representation of the θ data, and to scale them into the order of magnitude of $0 \div 1$, the following *momentum thickness parameter* θ^* is introduced:

$$\theta^* = 100 \cdot (c/c_t) \cdot F(D) \tag{4}$$

The combination of formulae (2) to (4) reads the following approximation:

$$P \propto \theta^* \tag{5}$$

In addition to the trend expressed by formula (5), it is also considered that, according to Lieblein (1965), the total pressure loss is proportional to the wake momentum thickness. These two proportionalities imply that a) a correlation exists between local loss and noise, b) the momentum thickness parameter θ^* is a simultaneous indicator of *both local loss and local noise* .

The majority of loss, represented herein by θ^*, develops on the suction surface of the blade, as discussed in Vad (2011). The blade suction sides "face" toward the US direction. Therefore, only the US PAM measurement data have been judged herein as being representative for any correlation between local loss and noise. As the US distributions in Fig. 2 suggest, the aerodynamic noise of the rotor (at $R = 0.30 \div 1.00$) dominates over the noise of the driving electric motor (at $R = 0 \div 0.30$) along the dominant portion of blade span for the bands of $f_{mid} = 2000$, 2500 and 3150 Hz. For these cases, a clear distinction can be made between the rotor noise and the motor noise. At higher frequencies, the noise of the motor is comparable with or even dominates over the aerodynamic noise of the rotor: one cannot make a clear distinction between these two noise sources along the radius.

For the above reasons, a correlation between L_{PM} and the momentum thickness parameter θ^* has been sought only for the US measurements, and only for the bands of $f_{mid} = 2000$, 2500 and 3150 Hz. As noted in Section 5, these bands are dominated by the suction side boundary layer noise. They are the most significant herein from the viewpoint of human audition (conf. Benedek and Vad, 2014).

For a generalization of the approach in formula (5), the local P_M was assumed to increase monotonically with θ^*. The power test function of $P_1 = A_1 \cdot (\theta^*)^{B1}$, enabling a straightforward mathematical treatment, was *arbitrarily* constructed for checking the validity of this assumption. In order to make possible a direct comparison with the logarithmic L_{PM} level, this power function was logarithmized and multiplied by 20 (as applied in the sound pressure level), resulting in $L_{P1} = 20 \cdot \log_{10} P_1$. The *momentum thickness level* was introduced as $L_{\theta^*} = \log_{10}(\theta^*)$. With these considerations, and introducing further parameters A and B (derived from A_1 and B_1), L_{P1} can be written in the following form:

$$L_{P1} = A + B \cdot L_{\theta^*} \qquad\qquad (6)$$

If the frequency-dependent parameters A and B can be adjusted by such means that a fair agreement occurs between the measurement-based $L_{PM}(R)$ and the approximate $L_{P1}(R)$ distributions, the correlation between the local spanwise-resolved loss and noise data is justified. The US $L_{PM}(R)$ distributions, presented in Fig. 2, were approximated along the entire span with functions $L_{P1}(R)$ of suitably chosen A and B parameter values. The mathematical method of approximation is detailed in Benedek and Vad (2014). The $L_{P1}(R)$ distributions, performing a best fit to the US $L_{PM}(R)$ profiles, are presented in Fig. 2 for f_{mid} = 2000, 2500 and 3150 *Hz*, using dot symbols. The quantitative interpretation of the $L_{P1}(R)$ functions, and their role in redesign for simultaneous reduction of loss and noise, is reported in a future publication. At present, the sole intention of the authors is to visualize in Fig. 2 that a fair correlation exists between the US $L_{PM}(R)$ and $L_{P1}(R)$ profiles.

The following example is given for an envisaged redesign strategy aiming at simultaneously reducing US-radiated rotor noise and rotor loss. The empirically determined A and B parameters are considered as redesign constants for each third-octave band for which the $L_{P1}(R)$ profile of Eq. (6) was found to correlate with the PAM-measured US noise. On this basis, Eq. (6) implies that the noise radiated from the annulus region can be reduced by moderating the L_{θ^*} values along the span. As Eqs. (3) and (4) read, the moderation of L_{θ^*} – i.e. the moderation of θ^* – at a given radius corresponds to a purposeful modification of the D and/or c values by redesign. The moderation of the momentum thickness, represented by θ^*, implies the reduction of total pressure loss as well (conf. Lieblein, 1965). When modifying D and/or c, a redesign constraint is that the global aerodynamic performance of the fan is to be retained. The following redesign possibilities are given for a purposeful modification of the D and/or c distributions along the span. a) Re-shaping the inlet cone, for obtaining a more favourable rotor inlet velocity condition. b) Re-shaping the rotor blading (e.g. chord modification, re-cambering, re-staggering). c) A combination of a) and b).

SUMMARY

Methodological improvement has been carried out in the recently elaborated technique aiming at combined acoustic-aerodynamic on-site diagnostics of industrial axial fans, with involvement of PAM experimentation and an in-house ROSI processing algorithm. The methodology has been demonstrated in a case study. The new results are summarized as follows.

1) A method has been presented for studying the effect of duration of averaging – or, analogously, the number of rotor revolutions of averaging – on the PAM results obtained by means of the ROSI algorithm. The third-octave band of the highest mid-frequency, being the most representative one from the viewpoint of turbulent fluctuations, has been found as the most relevant indicator of sensitivity to duration of averaging. PAM records were processed for three various durations of averaging, forming a geometric sequence with common ratio 2. The effect of duration of averaging has been visualized and interpreted in the form of *subtractive source maps*, generated by subtracting the individual maps related to the various durations. The range of the subtractive maps has been set to the range of uncertainty of the PAM measurements. It has been concluded that, by applying the longest duration (20 *s*, i.e. 480 revolutions, in the present case), an insensitivity of the PAM results is reached with respect to duration of averaging, within the range of measurement uncertainty.

2) In evaluating the source maps, it has been found ambiguous whether the noise peaks in the source maps are associated with flow phenomena related to the blade *preceding* or *following* the peaks with reference to the direction of rotation. The following technique, adaptable to on-site measurements, has been applied for eliminating such ambiguity. The tip clearance for a single blade has been reduced. This was carried out by means of attaching a narrow plate to the tip. The plate has a camber geometry being identical with that of the tip. The PAM measurements have been repeated, and the resultant source maps were compared with those related to uniform tip clearance. The qualitative changes in the noise peaks, observed consequently for each frequency band, were registered and interpreted. On this basis, it has been concluded that the noise peaks are associated with phenomena related to the blades *preceding* the peaks, in this particular case study.

3) The source maps have been evaluated in detail, involving the technique described in the previous point. On this basis, the concept of *double-leakage flow noise* has been introduced. The following noise sources have been identified: tip leakage flow noise – also incorporating double-leakage flow noise –; suction side boundary layer noise.

4) The *momentum thickness parameter* θ^* has been established as a representative indicator of both loss and US-radiated aerodynamic noise, along the span. The local θ^* values are calculated by straightforward arithmetical means, taking input data easily available from rotor geometry, as well as from preliminary rotor design and analysis, such as c and D. The *momentum thickness level* has been introduced, making possible a direct comparison with the logarithmic sound pressure level. The literature has been extended by comparing experiment-based, spanwise-resolved distributions of US sound pressure level and momentum thickness level. A fair correlation has been found between these two characteristics along the entire span, for the frequency bands being the most significant from the viewpoint of human audition within the investigated range. This correlation offers a basis for elaborating guidelines for redesign of the fan inlet and/or the rotor, for simultaneous reduction of noise and loss at a prescribed aerodynamic performance.

REFERENCES

Benedek, T., Vad, J. (2014), Concerted aerodynamic and acoustic diagnostics of an axial flow industrial fan, involving the phased array microphone technique. *ASME Paper* GT2014-25916.

Bianchi, S., Corsini, A., Rispoli, F., Sheard, A. G. (2009), Experimental aeroacoustic studies on improved tip configurations for passive control of noise signatures in low-speed axial fans. *ASME J. Vibration and Acoustics*, **131**, pp. 061007-1:061007:10.

Bianchi, S., Corsini, A., Rispoli, F., Sheard, A. G. (2011), Far-field radiation of tip aerodynamic sound sources in axial fans fitted with passive noise control features. *ASME J. Vibration and Acoustics*, **133**, pp. 051001-1:051001:11.

Carolus, T. (2003), *Ventilatoren*. Teubner Verlag, Wiesbaden.

Corsini, A., Bianchi, S., Sheard, A. G. (2009), Aerodynamic performance of blade tip end-plates designed for low-noise operation in axial flow fans. *ASME J.Fluids Engineering*, **131**(8), pp. 1-13.

Daly, B. B. (1992), *Woods practical guide to fan engineering* . Woods of Colchester Ltd. (sixth impression)

De Gennaro, M., Kuehnelt, H. (2012), Broadband noise modelling and prediction for axial fans. *Proc. International Conference on Fan Noise, Technology and Numerical Methods (FAN2012)* , Senlis, France, ISBN 978-0-9572374-1-4.

Fukano T., Jang C.-M. (2003), Tip clearance noise of axial flow fans operating at design and off-design condition. *J. Sound and Vibration* , **275**, pp. 1027-1050.

Hald, J., (2005), Combined NAH and beamforming using the same array. *Brüel & Kjær Technical Note* (2005-1)

Horváth, Cs., Envia, E., Podboy. G. G. (2014), Limitations of phased array beamforming in open rotor noise source imaging. *AIAA Journal*, **52**(8), pp. 1810-1817.

Ji L., Qiao W., Zhao L., Xu K., Wang L. (2013), An investigation of the inlet and exhaust noise sources of turbofan using linear microphone array. *AIAA Paper* 2013-2296.

Kennedy J., Eret P., Bennett G., Sopranzetti F., Chiariotti P., Castellini P., Finez A., Picard C. (2013), The application of advanced beamforming techniques for the noise characterization of installed counter rotating open rotors. *AIAA Paper* 2013-2095.

Khalid, S. A., Khalsa, A. S., Waitz, I. A., Tan, C. S., Greitzer, E. M., Cumpsty, N. A., Adamczyk, J. J., Marble, F. E. (1999), Endwall blockage in axial compressors. *ASME J. Turbomachinery* , **121**, pp. 499-509.

Lakshminarayana, B. (1996), *Fluid Dynamics and Heat Transfer of Turbomachinery* . John Wiley & Sons, Inc.

Lieblein, S. (1965), Experimental flow in two-dimensional cascades. Chapter VI in *Aerodynamic design of axial-flow compressors* . NASA SP-36, Washington D. C.

Lowis, C., Joseph, P. (2006), Determining the strength of rotating broadband sources in ducts by inverse methods. *J. Sound and Vibration* , **295** (3-5), pp. 614-632.

Minck, O., Binder, N., Cherrier, O., Lamotte, L., Budinger, V. (2012), Fan noise analysis using a microphone array. *Proc. International Conference on Fan Noise, Technology and Numerical Methods (FAN2012)* , Senlis, France, ISBN 978-0-9572374-1-4.

Mueller, T., Allen, C., Blake, W. K., Dougherty, R. P., Lynch, D., Soderman, P., Underbrink, J. (2002), *Aeroacoustic measurements* . Springer (first edition)

Podboy, G. G., Horváth, Cs. (2009), Phased array noise source localization measurements made on a Williams International FJ44 engine. *AIAA Paper* 2009-3183.

Ristrorcelli, J. R. (1997), A pseudo-sound constitutive relationship for the dilatational covariances in compressible turbulence. *Journal of Fluid Mechanics* , **347**, pp. 37-70.

Shin, H., Graham, W., Sijtsma, P., Andreou, C., Faszer, A. (2007), Implementation of a phased microphone array in a closed-section wind tunnel. *AIAA Journal*, **45**(12), pp. 2897–2909.

Sijtsma, P., Oerlemans, S. Holthusen, H. (2001), Location of rotating sources by phased array measurements. *AIAA Paper* 2001-2167.

Sijtsma, P. (2010), Using phased array beamforming to identify broadband noise sources in a turbofan engine. *Int. J. Aeroacoustics* , **9** (3), pp. 357-374.

Vad, J. (2011), Correlation of flow path length to total pressure loss in diffuser flows. *Proc. IMechE, Part A – J. Power and Energy* , **225**, pp. 481-496.